REDISCUSSION OF ECLIPSING BINARIES. PAPER X. THE PULSATING B-TYPE SYSTEM V1388 ORIONIS

By John Southworth[1] *and Dominic M. Bowman*[2]

1. *Astrophysics Group, Keele University, Staffordshire, ST5 5BG, UK*
2. *Institute of Astronomy, KU Leuven, Celestijnenlaan 200D, B-3001 Leuven, Belgium*

V1388 Ori is an early-B type detached eclipsing binary whose physical properties have previously been measured from dedicated spectroscopy and a ground-based survey light curve. We reconsider the properties of the system using newly-available light curves from the Transiting Exoplanet Survey Satellite (*TESS*). We discover two frequencies in the system, at 2.99 d^{-1} and 4.00 d^{-1} which are likely due to β Cephei or SPB pulsations. We are not able to find a fully satisfactory model of the eclipses, but the best attempts show highly consistent values for the fitted parameters. We find masses of 7.24 ± 0.08 $M_\odot$ and 5.03 ± 0.04 $M_\odot$, and radii of 5.30 ± 0.07 $R_\odot$ and 3.14 ± 0.06 $R_\odot$. The properties of the system are in good agreement with theoretical predictions and the *Gaia* EDR3 parallax if the published temperature estimates are revised downwards by 1500 K, to 19 000 K for the larger and more massive star and 17 000 K for its companion.

Introduction

Detached eclipsing binaries (dEBs) are our primary source of measurements of the physical properties of normal stars[1–3]. Those containing high-mass stars are of particular importance because such stars dominate the light of young stellar populations[4,5] and the chemical evolution of galaxies[6], and give rise to a wide variety of exotic objects[7–10]. Theoretical models of massive stars remain limited by the imperfect understanding of several phenomena including internal mixing and convective core overshooting[11,12], angular momentum transport[13] and the effects of internal gravity waves[14,15]. Massive stars are typically found in multiple systems[16,17], and their evolution is dominated by binary interactions[18].

In this work we revisit the V1388 Ori system (Table I), using a recently-obtained space-based light curve, with the aim of determining its physical properties to high precision[19]. It was classified as a B2 V star by Walborn[20] and has been used as a spectral standard star[21], before the discovery of eclipses in its light curve from the *Hipparcos* satellite[22,23]. A detailed study of V1388 Ori was presented by Williams[24] (hereafter W09) based on 29 coudé spectra (resolving power $R = 11\,500$) and a scattered V-band light curve from the All Sky Automated Survey (ASAS, Pojmański[25,26]). W09 used the ELC code[27] to fit the light and radial velocity (RV) curves and measure the properties of the system. They also determined effective temperature ($T_{\rm eff}$) values of $20\,500 \pm 500$ K and $18\,500 \pm 500$ K for the two stars.

Table I: *Basic information on V1388 Ori.*

Property	*Value*	*Reference*
Henry Draper designation	HD 42401	[28]
Hipparcos designation	HIP 29321	[22]
Tycho designation	TYC 738-244-1	[29]
Gaia EDR3 designation	3342421035256268544	[30]
Gaia EDR3 parallax	1.3198 ± 0.0432 mas	[30]
TESS Input Catalog designation	TIC 337165095	[31]
B magnitude	7.424 ± 0.015	[29]
V magnitude	7.493 ± 0.018	[29]
J magnitude	7.506 ± 0.024	[32]
H magnitude	7.541 ± 0.027	[32]
K_s magnitude	7.551 ± 0.034	[32]
Spectral type	B2 V	[20]

Observational material

V1388 Ori has been observed on three occasions by the NASA *TESS* satellite[33]. It was observed in long cadence (600 s sampling rate) in sector 33 (2020/12/17 to 2021/01/13) but we did not use these data due to their coarser temporal sampling. It was observed in short cadence (120 s sampling rate) in sectors 43 (2021/09/16 to 2021/10/12) and 45 (2021/11/06 to 2021/12/02), and these data were analysed for this work.

We downloaded the data from the MAST archive* and converted the fluxes to relative magnitude. We retained only those observations with a QUALITY flag of zero, leaving 32 307 of the original 35 893 datapoints. The simple aperture photometry (SAP) and pre-search data conditioning SAP (PDCSAP) data[34] were visually almost indistinguishable, the only clear differentiating feature being a 0.002 mag variation in eclipse depth. We therefore adopted the SAP data as usual in this series of papers, and ensured that we fitted for third light in the analysis below. The light curve is shown in Fig. 1.

Initial analysis of the light curve

The components of V1388 Ori are significantly distorted due to their large fractional radii ($r_{\rm A}$ and $r_{\rm B}$ where $r_{\rm A} = R_{\rm A}/a$, $r_{\rm B} = R_{\rm B}/a$, $R_{\rm A}$ and $R_{\rm B}$ are the radii of the stars, and a is the semimajor axis of the relative orbit) so the light curve must be analysed using a model incorporating Roche geometry. However, this is time-intensive due to the large calculation time required to model a large number of datapoints using existing Roche-geometry codes. We therefore performed a preliminary analysis with the JKTEBOP† code[35,36] in order to determine the orbital ephemeris of the system, thus allowing us to convert all the data to orbital phase and bin into a small number of phased datapoints.

*Mikulski Archive for Space Telescopes, `https://mast.stsci.edu/portal/Mashup/Clients/Mast/Portal.html`

†`http://www.astro.keele.ac.uk/jkt/codes/jktebop.html`

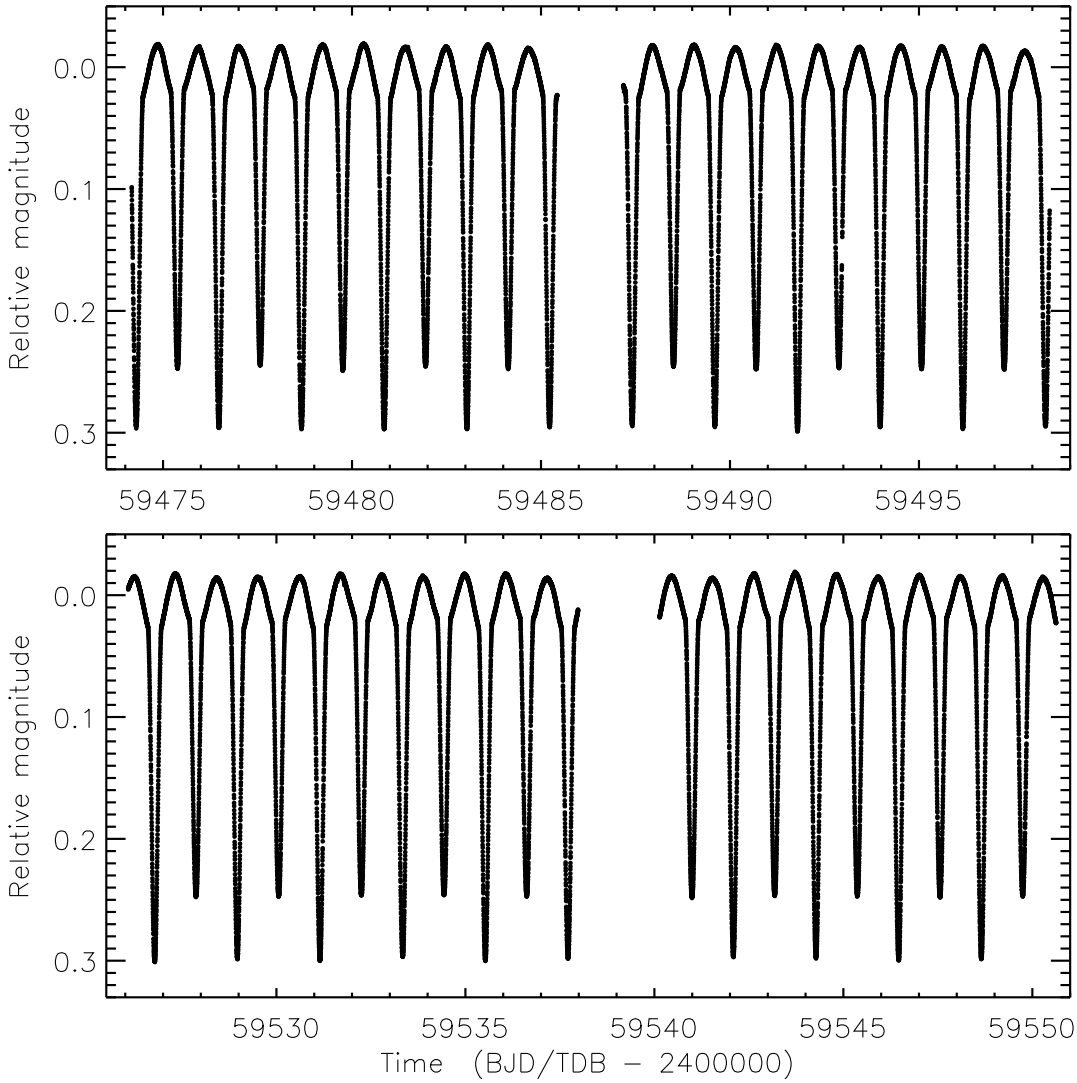

Figure 1: *TESS* short-cadence SAP photometry of V1388 Ori from sectors 43 (top panel) and 45 (bottom panel). The flux measurements have been converted to relative magnitude and rectified to zero magnitude by subtraction of low-order polynomials.

We fitted the full *TESS* sector 43 and 45 light curve with JKTEBOP, assuming a circular orbit. We defined star A to be that eclipsed at primary minimum, making it the hotter of the two components (and also the larger and more massive component in the case of V1388 Ori), and star B to be its companion. After obtaining a preliminary orbital ephemeris, we checked it against the time of inferior conjunction from W09[‡]. That timing was converted from the UTC timescale to TDB using the IDL routines of Eastman *et al.*[37]. The resulting ephemeris for primary minimum (based only on the *TESS* data) is

$$\text{Min I} = \text{BJD/TDB } 2459485.226609(16) + 2.18703006(82)E \qquad (1)$$

[‡]W21 quote their reference time using the notation $T_{\rm IC,1}$ to denote the "time of inferior conjunction of the primary star". However, they also note that "this is the time of secondary minimum in the light curve". The two statements are in mutual conflict. Using our preliminary ephemeris we determined that the $T_{\rm IC,1}$ value in W09 is indeed a time of secondary eclipse, and therefore it it a time of *superior* conjunction of star A.

where E is the cycle number since the reference time and the bracketed quantities indicate the uncertainties in the last digit of the preceding number. There is a small amount of tension between the ephemerides based on the individual *TESS* sectors, both with and without the timing from W09, suggesting that the orbital period of V1388 Ori is not constant. This does not affect the following analysis, but it is worth investigation in future.

Armed with this ephemeris, we converted each of the *TESS* sector 43 and 45 light curves into orbital phase and binned them into 400 points equally distributed over phases 0 to 1. The two binned light curves look almost identical. As a check, we phase-binned the PDCSAP data as well, and found that the slightly larger eclipse depths in the PDCSAP data occurred in both *TESS* sectors.

Frequency analysis

Following previous work on massive pulsators in eclipsing binaries[38], the residuals of the JKTEBOP fit to the unbinned SAP data were used to search for the presence of pulsations in V1388 Ori. We used the combined sectors 43 and 45 residual light curve and calculated the discrete Fourier transform[39]. There are many significant peaks in the resultant amplitude spectrum, but almost all of them fall at integer multiples of the orbital frequency. Therefore, they likely do not represent independent pulsation mode frequencies, but are rather a consequence of an imperfect binary model leaving residual signal at orbital harmonics (see below).

However, we detected two significant frequencies that do not coincide with orbital harmonics, namely 2.9943 ± 0.0002 d^{-1} and 3.9987 ± 0.0004 d^{-1}. We define *significant* to mean that the signal-to-noise ratio (S/N) is larger than five in the amplitude spectrum after all orbital harmonics have been removed, using a 1 d^{-1} frequency window in the amplitude spectrum centred on the extracted frequency to estimate the local noise level. Additional variability at lower frequency is visually evident, but has S/N < 4 so formally falls below our detection threshold and is not significant. These frequencies are typical of β Cephei or SPB (slowly-pulsating B-star) pulsation modes[40–42]. The spectral type of V1388 Ori is consistent with such pulsations, so we conclude that the system is a new example of a massive pulsator in a dEB. Such systems are rare and could provide useful probes of stellar interiors through forward asteroseismic modelling.

Fig. 2 shows the amplitude spectrum of the residuals of the JKTEBOP fit to the unbinned SAP data. A large number of frequencies are present at multiples of the orbital frequency ($f_{\rm orb} = 0.45724$ d^{-1}). The highest-frequency of these is at $60 f_{\rm orb}$ (not shown on the plot). The two significant frequencies are indicated in Fig. 2 using arrows.

A Roche-geometry model of the light curve

The light curve binned into 400 points in orbital phase was modelled using the Wilson-Devinney code[43,44], in order to determine the photometric properties of the system. We used the 2004 version of the code (WD2004) driven by the

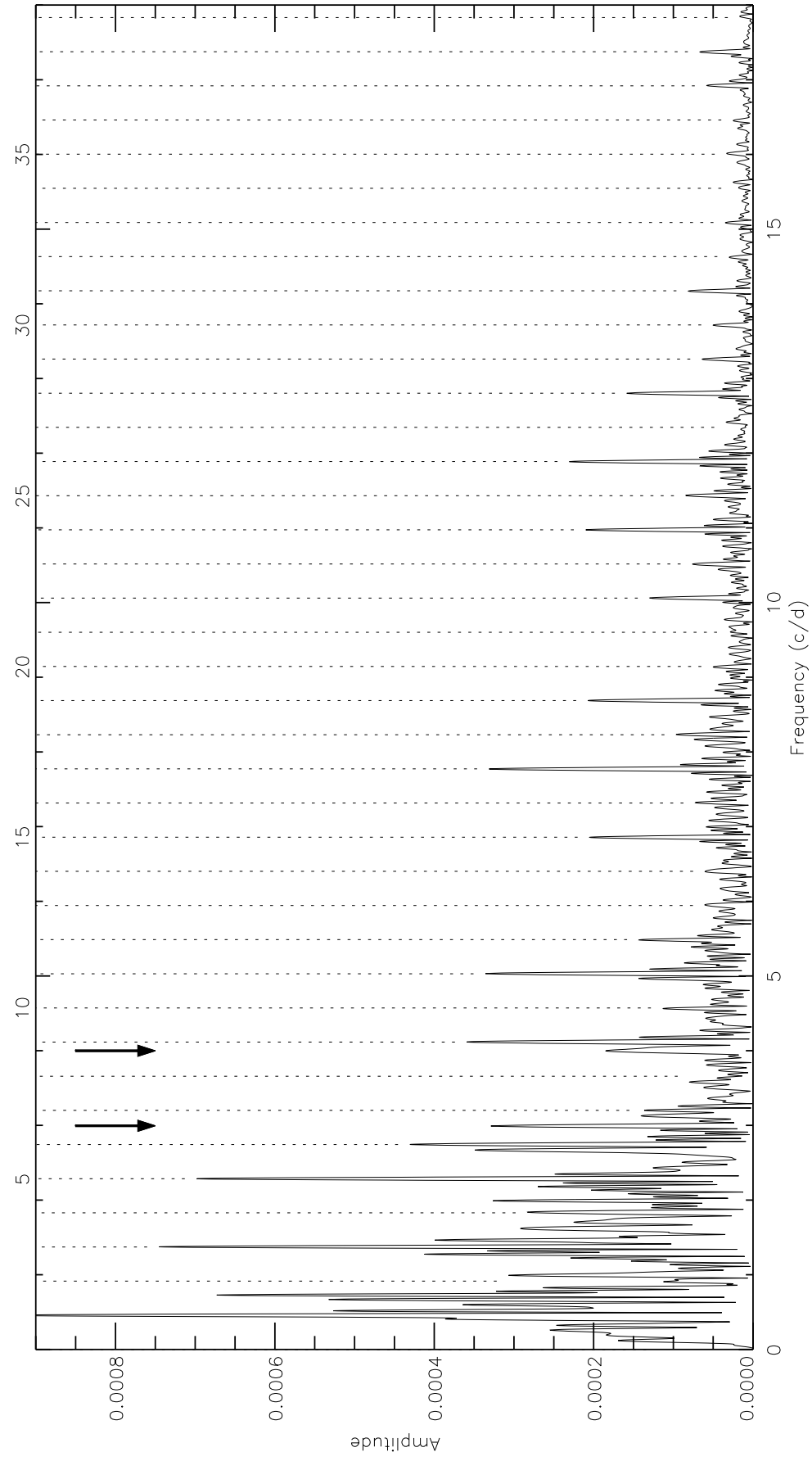

Figure 2: Amplitude spectrum of the *TESS* light curve of V1388 Ori after subtraction of the JKTEBOP binary model. The dotted lines indicate multiples of the orbital frequency, and the multiplicative factor is given above the top of the plot for each fifth factor. The arrows indicate the two frequencies that are significantly detected and do not coincide with orbital harmonics.

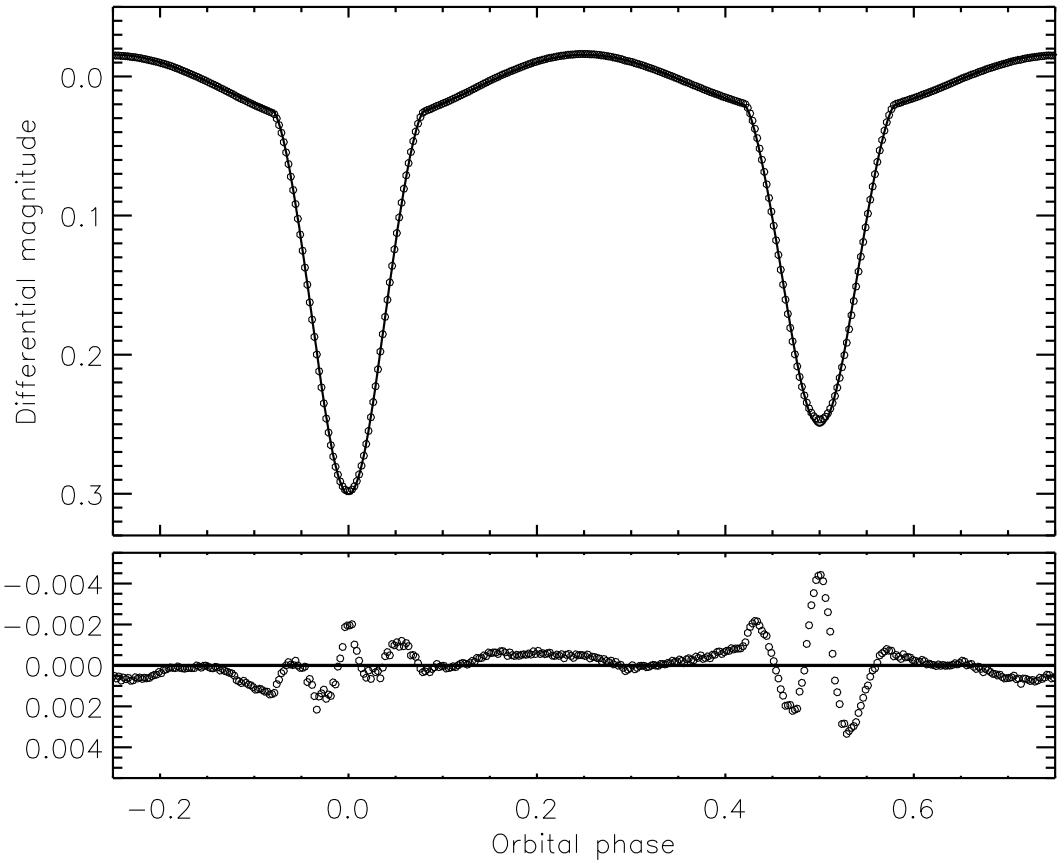

Figure 3: Best fit to the binned light curve of V1388 Ori using WD2004. The phase-binned data are shown using open circles and the best fit with a continuous line. The residuals are shown on an enlarged scale in the lower panel.

JKTWD wrapper[45]. WD2004 uses Roche geometry to accurately model the light curves of distorted stars in close binary systems.

We have not been able to get a good fit to the light curve. Our best attempt is shown in Fig. 3 and has significant residuals, as large as 4 mmag, through both eclipses. The reason for this remains unclear, as we have not encountered this precise problem in previous work on similar or different binary systems[19,38,46–48]. In what follows we discuss the default setup of the modelling process and our attempts to improve the fit.

Operation mode. The two relevant choices in WD2004 are mode 0 ($T_{\rm eff}$ values and light contributions are not forced to be consistent) and mode 2 (the $T_{\rm eff}$ values and passband-specific light contributions are forced to be consistent via the use of tabulated predictions from stellar model atmospheres). In our default approach we used mode 0, fixed the $T_{\rm eff}$ values at those from W09, and directly fitted for the contributions of the two stars to the total light of the system. As an alternative we chose mode 2 and fitted for the $T_{\rm eff}$ of star B, finding a very similar value (18 424 versus 18 500 K) and a similar quality of fit. We used a Johnson R passband as the closest available option to the *TESS* band, but obtained practically identical results with a Johnson I passband.

Numerical precision. Our inital solutions were performed with a low numerical

precision of `N1=N2=30` (see the WD2004 user guide[49]). Increasing this to the maximum value of 60 allowed a slight improvement in the fit.

Mass ratio. We fixed the mass ratio at the value of 0.695 ± 0.003 measured spectroscopically by W09. The alternative approach of fitting for this quantity gives a better fit to the light curve but a mass ratio, 0.539, which is quite discrepant with the spectroscopic value.

Orbital eccentricity. V1388 Ori is expected to have a circular orbit due to its age (W09) and short tidal timescales[50,51]. However, a small eccentricity does give more freedom to fit eclipse profiles because it allows the primary and secondary eclipses to have different impact parameters. If the argument of periastron, ω, is set to 90° or 270° it is possible to have an eccentric orbit where the secondary eclipse is still at phase 0.5. We tried this but were unable to significantly improve the fit. All solutions prefer at most a small eccentricity (0.01 or less) and there is no clear evidence for non-circularity.

Rotation rate. Tidal effects are also expected to have caused the rotation of the stars to synchronise with the orbital motion, so in our default solution we assumed synchronous rotation. Attempts to fit the rotation rate of star B failed because it has a negligible effect on the shape of the light curve. Fitting for the rotation rate of star A yielded a determinate solution for faster rotation (1.7 times the synchronous value) but an only slightly improved fit. W09 measured the rotational velocities of the two stars from their spectral line profiles, finding them to be consistent with synchronous rotation.

Albedo. We were able to find a significantly better model of the *TESS* light curve by fitting for the albedos of the two stars. The residuals decreased from 0.96 mmag to 0.51 mmag and the residuals during eclipse became much smaller (Fig. 4). However, the fitted values of the albedo are 4.8 and 4.5, so are physically unrealistic[52]. Such a large albedo would require the stars to emit much more light in the *TESS* passband than is incident on them. We have seen a similar problem in the past (e.g. KIC 10661783[53–55]) and suspect that it arises due to a physical effect not included in the WD2004 model. For our default values we therefore fixed the albedos of both stars to 1.0.

Gravity darkening. Both components are expected to have a gravity darkening exponent of $\beta = 1.0$ (Ref.[56]). A significantly improved fit can be obtained by specifying values very different from this; a straight fit returns $\beta = -7.7$ for star B, which must be rejected on physical grounds.

Reflection effect. WD2004 includes the option of a detailed treatment of the reflection effect[57] which we normally do not use because of the additional computing time needed. Use of the detailed treatment caused no improvement in the quality of the fit.

Third light. A small amount of third light is expected to be common in data from *TESS* because of the large pixel size (21″). We included this parameter by default and consistently obtained a small negative value. This is physically plausible if the background subtraction in the data reduction process is imperfect, and has been seen before in a similar system[58].

Limb darkening (LD). Our original fits used the linear LD law and coefficients fixed at values interpolated from the tables of Van Hamme[59]. Use of the square-

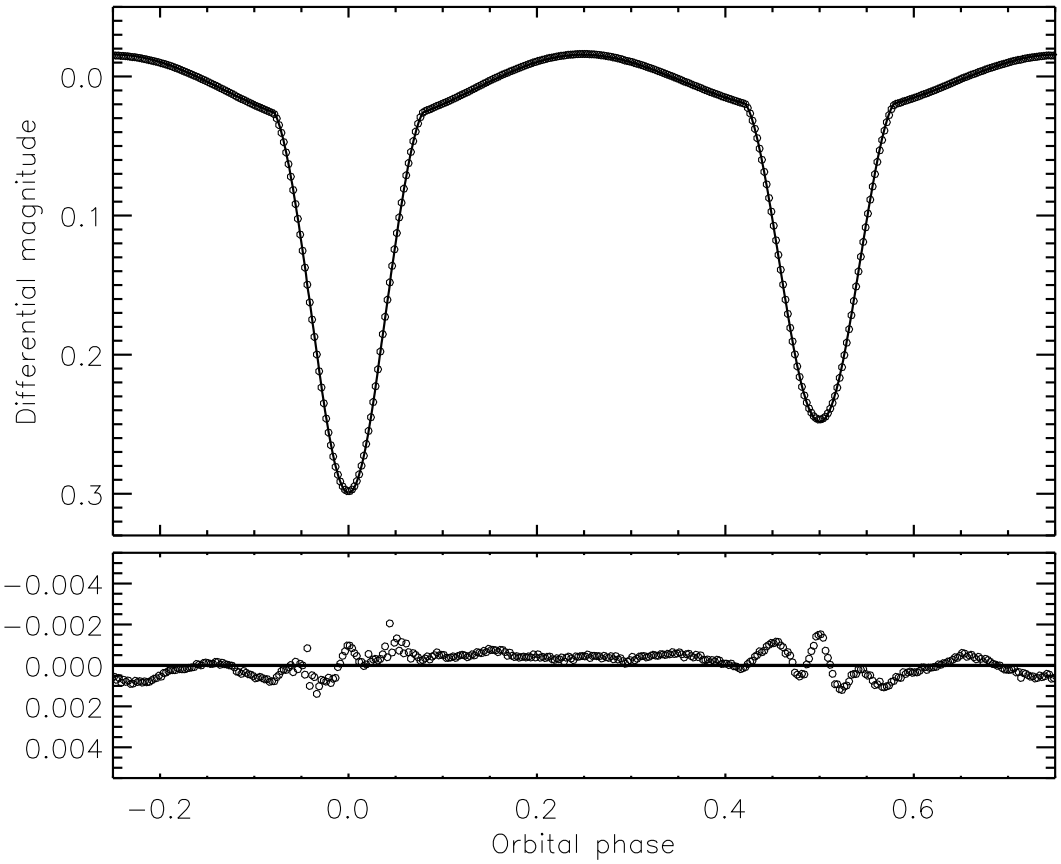

Figure 4: Same as for Fig. 3 except for a solution where the albedos of the two stars were fitted.

root or logarithmic LD laws gave almost identical results. Fitting for one LD coefficient per star allowed a small improvement in the fit. For our final fits we assumed logarithmic LD and fitted for the coefficients.

Inverted ratio of the radii. It is often possible to get relatively good fits to the light curve of a dEB for both a certain ratio of the radii ($k = r_{\rm B}/r_{\rm A}$) and its reciprocal ($1/k$). We were indeed able to locate a solution with $k > 1$ for V1388 Ori, but the quality of the fit was significantly worse and the values of the fitted LD coefficients were very different from theoretical predictions. The $k > 1$ solution is also discrepant with the spectroscopic light ratio measured by W09.

Data reduction. We obtained a fit to the PDCSAP data to compare to the default solution using the SAP data. The measured parameter values and residuals were almost identical between the two fits.

Subsections of the light curve. We fitted the sector 43 and sector 45 light curves separately, finding that the two solutions were extremely similar. The behaviour of V1388 Ori is therefore consistent over a time interval of at least 76 d.

Final model of the light curve

In light of the problems outlined above, we abandoned our attempts to get a *good* fit to the light curve and settled for merely the *best* fit, from the point of

Table II: *Summary of the parameters for the* WD2004 *solution of the TESS light curve of V1388 Ori. Uncertainties are only quoted when they have been assessed by comparison between a full set of alternative solutions.*

Parameter	*Star A*	*Star B*
Control parameters:		
WD2004 operation mode	0	
Treatment of reflection	1	
Number of reflections	1	
Limb darkening law	2 (logarithmic)	
Numerical grid size (normal)	60	
Numerical grid size (coarse)	60	
Fixed parameters:		
Mass ratio	0.695	
Rotation rates	1.0	1.0
Bolometric albedos	1.0	1.0
Gravity darkening	1.0	1.0
$T_{\rm eff}$ values (K)	20 500	18 500
Bolometric linear LD coefficient	0.5494	0.5760
Bolometric logarithmic LD coefficient	0.2339	0.2184
Passband logarithmic LD coefficient	0.5124	0.4881
Fitted parameters:		
Phase shift	-0.00003 ± 0.00002	
Potential	3.843 ± 0.030	4.788 ± 0.066
Orbital inclination (°)	77.50 ± 0.33	
Orbital eccentricity	0.0 fixed	
Light contributions	10.11 ± 0.27	2.90 ± 0.11
Passband linear LD coefficient	0.24 ± 0.14	0.12 ± 0.20
Third light	-0.032 ± 0.023	
Derived parameters:		
Light ratio	0.287 ± 0.013	
Fractional radii	0.3242 ± 0.0022	0.1923 ± 0.0034

view of low residuals whilst remaining physically reasonable. Our final parameter values are based on fitting the phase-binned sector 43 light curves using WD2004 in mode 0, the simple reflection effect, the maximum numerical grid size of 60, a circular orbit, and the logarithmic LD law. The fitted parameters were the potentials of the two stars, the orbital inclination, the linear LD coefficient for each star, the phase of primary minimum, the light contributions of the two stars, and third light. The results are given in Table II.

To determine the uncertainties in the fitted parameter values we ran new fits with different input parameters or approachs. These fits comprised: changing the mass ratio by ± 0.003; changing the rotation rate by ± 0.1, changing the albedo by ± 0.1; changing the gravity darkening exponents by ± 0.1; a numerical grid size of 40 instead of 60, use of mode 2 instead of 0, use of the detailed reflection effect; and linear instead of logarithmic LD. For each we calculated the changes in the values of the fitted parameters, then added these changes in quadrature

to obtain the full errorbars for the parameters. We also considered fits with the LD coefficients fixed at the theoretical values instead of fitted for, and with third light fixed at zero, but in both cases the residuals were significantly higher so we did not include the results in the errorbars. The uncertainties reported by the differential-corrections fitting algorithm in WD2004 are in all cases much smaller than the uncertainties quoted in Table II.

The fractional radii, $r_{\rm A}$ and $r_{\rm B}$, are the most useful results in Table II. $r_{\rm A}$ is highly consistent between alternative fits so is precisely determined. $r_{\rm B}$ varies more, the biggest differences being seen for numerical precision and a change of gravity darkening exponent. As we were not able to get a good fit to the data, the uncertainty in $r_{\rm A}$ in Table II should be seen as a lower limit. In the following analysis we accounted for this by doubling the errorbar. It was not necessary to do the same for $r_{\rm B}$ because its errorbar was already significantly larger.

The light ratio in Table II, $\ell_2/\ell_1 = 0.287 \pm 0.013$, is in excellent agreement with the spectroscopic value of 0.25 ± 0.05 determined by W09. That it is slightly (although not significantly) higher is expected because the *TESS* passband (approximately 590–990 nm) is redder than the blue wavelength range covered by W09's spectra (425–457 nm).

Physical properties of V1388 Ori

We have calculated the physical properties of the V1388 Ori system using the $r_{\rm A}$, $r_{\rm B}$ and orbital inclination from Table II, with the errorbar on $r_{\rm A}$ doubled. To this we added the period found above and velocity amplitudes of $K_{\rm A} = 151.4 \pm 0.3$ km s^{-1} and $K_{\rm A} = 217.9 \pm 1.0$ km s^{-1} from W09. The calculations were performed with the JKTABSDIM code[60]. To determine the distance to the system we used the apparent magnitudes given in Table I, bolometric corrections from Girardi *et al.*[61], and an interstellar extinction of $E(B-V) = 0.18 \pm 0.09$ mag from the STILISM[§] online tool[62,63]. The results are given in Table III. The 2MASS JHK_s magnitudes were obtained at a convenient orbital phase of 0.408 so represent the brightness of the system shortly before the start of secondary eclipse.

We have measured the masses and radii of the two stars to precisions of 1.8% or better, so they are suitable for inclusion in the Detached Eclipsing Binary Catalogue (*DEBCat*[¶], Ref.[65]). We find slightly smaller masses than did W09 (7.24 ± 0.08 and 5.03 ± 0.04 M$_\odot$ versus 7.42 ± 0.08 and 5.16 ± 0.03 M$_\odot$), but only because our measurement of the orbital inclination is higher. More interestingly, our radius measurements are much lower: 5.30 ± 0.07 and 3.14 ± 0.06 R$_\odot$ versus W09's 5.60 ± 0.04 and 3.76 ± 0.03 R$_\odot$. Our results are based on a *TESS* light curve incomparably better than the ASAS data available to W09, so should be preferred; the errorbars in the published measurements look too small. Although we were not able to find a good fit to the *TESS* data, the residuals are much smaller than the scatter of the ASAS data so it is reasonable to expect that both datasets suffer from the problem. Our preferred distance measurement is

[§] `https://stilism.obspm.fr`

[¶] `https://www.astro.keele.ac.uk/jkt/debcat/`

Table III: *Physical properties of V1388 Ori defined using the nominal solar units given by IAU 2015 Resolution B3 (Ref.[64]). The $T_{\rm eff}$ values are from W09.*

Parameter	*Star A*	*Star B*
Mass ratio	0.6948 ± 0.0035	
Semimajor axis of relative orbit ($\mathcal{R}^{\rm N}_\odot$)	16.352 ± 0.051	
Mass ($\mathcal{M}^{\rm N}_\odot$)	7.237 ± 0.078	5.028 ± 0.038
Radius ($\mathcal{R}^{\rm N}_\odot$)	5.301 ± 0.074	3.144 ± 0.056
Surface gravity (log[cgs])	3.849 ± 0.012	4.144 ± 0.015
Density ($\rho_\odot$)	0.0486 ± 0.0020	0.1617 ± 0.0086
Synchronous rotational velocity (km s^{-1})	122.6 ± 1.7	72.7 ± 1.3
Effective temperature (K)	19000 ± 1000	17000 ± 1000
Luminosity $\log(L/\mathcal{L}^{\rm N}_\odot)$	3.650 ± 0.044	3.018 ± 0.049
$M_{\rm bol}$ (mag)	-4.39 ± 0.11	-2.81 ± 0.12
Distance (pc)	759 ± 23	

from the K_s band, and is consistent with those from the other bands. Our initial distance measurement (see below) was 791 ± 24 pc, 1.1σ longer than the parallax-based distance of 757 ± 25 pc from *Gaia* EDR3.

To investigate these discrepancies, we have compared our measurements of V1388 Ori to theoretical predictions from the PARSEC stellar evolutionary code[66]. We did this in mass–radius and mass–$T_{\rm eff}$ parameter space as these are good diagnostic plots[46]. We find that the masses and radii of the stars are matched by predictions for an age of 33 ± 2 Myr and a heavy-element abundance of $Z = 0.020$. This is probably consistent with solar abundance considering recent developments[67–69]. Their $T_{\rm eff}$ values are higher than predicted by approximately 1500 K, which corresponds to slightly less than the difference between the B2 V and B2.5 V spectral type[70]. If we lower the $T_{\rm eff}$ values by this amount, we find a distance to the system of 759 ± 23 pc that is in almost perfect agreeement with *Gaia* EDR3. This represents our preferred set of system parameters as specified in Table III. A comparison with other similar sets of theoretical models[71,72] led to the same conclusions. The comparison is shown graphically in Fig.5.

We then performed the same comparison but with the system properties from W09. We found a rough agreement for $Z = 0.060$ and an age of 22 Myr, but even this extremely high metallicity (the highest available in PARSEC) underpredicted the radius and $T_{\rm eff}$ of star B by approximately 3σ and 2σ, respectively. We conclude that the published properties for this system are inconsistent with current stellar evolutionary models. W09 showed a Hertzsprung-Russell diagram (their fig. 7) in which the stellar properties agreed with the Lejeune & Schaerer[73] isochrones for an age of 25 Myr, but the stars were significantly too massive to match the predictions from Schaller *et al.*[74] (a situation also noticed by W09). This highlights how a decent agreement in a HR diagram is not sufficient for dEBs because mass is not directly involved; the use of mass–radius and mass–$T_{\rm eff}$ plots (Fig. 5) is better as it allows conclusions to be drawn both more easily and more robustly.

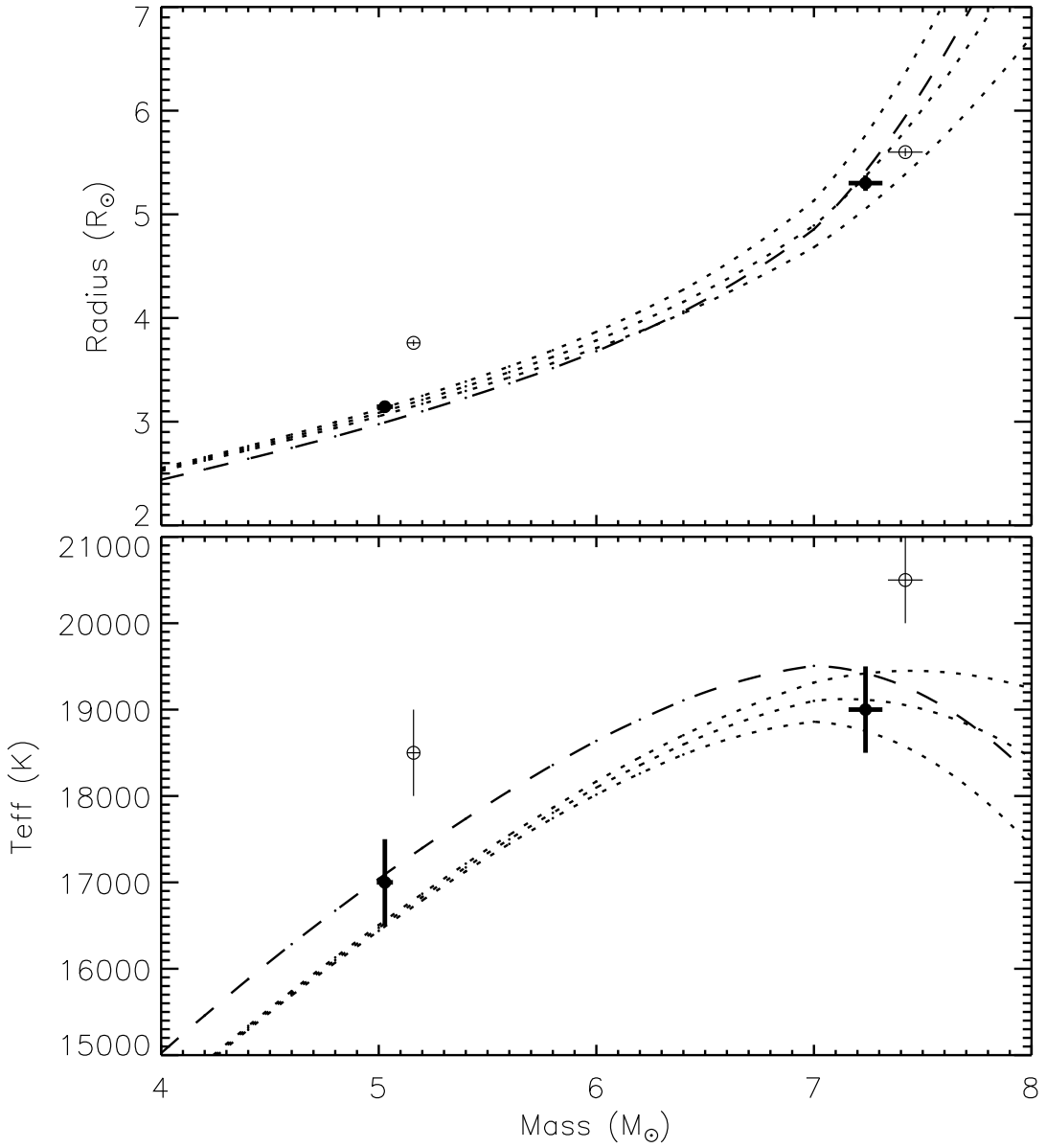

Figure 5: Mass–radius and mass–$T_{\rm eff}$ plots showing the properties of V1388 Ori versus predictions from the PARSEC models[66]. The dotted lines are model predictions for $Z = 0.020$ and ages of 31, 33 and 35 Myr. The dashed lines are predictions for $Z = 0.014$ and an age of 35 Myr. The filled circles with thick errorbars show the properties determined in the current work. The open circles with thin errorbars show the values found by W09.

Summary and conclusions

V1388 Ori is a dEB containing two early-B stars with significant tidal distortions. We used the *TESS* light curve and published spectroscopic results to study the system. The residuals of the fit of an eclipsing binary model to the *TESS* data were used to obtain a frequency spectrum. We detected two significant pulsation frequencies in the system which could be due to β Cephei or SPB star pulsation modes, making V1388 Ori one of the few known dEBs containing

stars that show these types of pulsation. The frequency spectrum also shows a large number of peaks at integer multiples of the orbital frequency.

We modelled the *TESS* light curve using the WD2004 code to determine the photometric parameters of the system. We were unable to obtain a good fit and, after extensive investigation, do not know why. Possible answers are an effect of the pulsations, issues with the data reduction process, or the presence of surface inhomogeneities on the stars. Despite this, the best model of the *TESS* data is very well constrained and appears to be a significant improvement on previous work.

By making the assumption that the results of the Roche-model analysis above are reliable, and using published velocity amplitudes, we determined the physical properties of the component stars. These are in good agreement with theoretical predictions and with the *Gaia* EDR3 parallax for an approximately solar metal abundance and an age of 33 Myr, if a small decrease in the published $T_{\rm eff}$ values of the stars is applied. A previous analysis of the system (W09), using much more limited photometry, returned radius measurements in poor agreement with our own and with theoretical predictions. A new spectroscopic study of this system would be useful to check if the lower $T_{\rm eff}$ values we find are reasonable.

Acknowledgements

This paper includes data collected by the *TESS* mission and obtained from the MAST data archive at the Space Telescope Science Institute (STScI). Funding for the *TESS* mission is provided by the NASA's Science Mission Directorate. STScI is operated by the Association of Universities for Research in Astronomy, Inc., under NASA contract NAS 5–26555. The following resources were used in the course of this work: the NASA Astrophysics Data System; the SIMBAD database operated at CDS, Strasbourg, France; and the arχiv scientific paper preprint service operated by Cornell University.

References

1 J. Andersen, *A&ARv*, **3**, 91, 1991.
2 G. Torres, J. Andersen & A. Giménez, *A&ARv*, **18**, 67, 2010.
3 J. Southworth, in *Living Together: Planets, Host Stars and Binaries* (S. M. Rucinski, G. Torres & M. Zejda, eds.), 2015, *Astronomical Society of the Pacific Conference Series*, vol. 496, p. 321.
4 D. F. de Mello, C. Leitherer & T. M. Heckman, *ApJ*, **530**, 251, 2000.
5 B. E. Robertson *et al.*, *Nature*, **468**, 49, 2010.
6 N. Langer, *ARA&A*, **50**, 107, 2012.
7 P. Podsiadlowski, S. Rappaport & E. D. Pfahl, *ApJ*, **565**, 1107, 2002.
8 P. Podsiadlowski *et al.*, *ApJ*, **607**, L17, 2004.
9 K. Belczynski *et al.*, *A&A*, **636**, A104, 2020.
10 A. A. Chrimes, E. R. Stanway & J. J. Eldridge, *MNRAS*, **491**, 3479, 2020.
11 A. Tkachenko *et al.*, *A&A*, **637**, A60, 2020.
12 C. Johnston, *A&A*, **655**, A29, 2021.
13 C. Aerts, S. Mathis & T. M. Rogers, *ARA&A*, **57**, 35, 2019.
14 D. M. Bowman *et al.*, *A&A*, **621**, A135, 2019.
15 D. M. Bowman *et al.*, *A&A*, **640**, A36, 2020.

16 H. Sana *et al.*, *ApJS*, **215**, 15, 2014.
17 H. A. Kobulnicky *et al.*, *ApJS*, **213**, 34, 2014.
18 H. Sana *et al.*, *Science*, **337**, 444, 2012.
19 J. Southworth, *The Observatory*, **140**, 247, 2020.
20 N. R. Walborn, *ApJS*, **23**, 257, 1971.
21 N. R. Walborn & E. L. Fitzpatrick, *1990PASP..102..379W*.
22 ESA (ed.), *The Hipparcos and Tycho catalogues. Astrometric and photometric star catalogues derived from the ESA Hipparcos space astrometry mission*, *ESA Special Publication*, vol. 1200, 1997.
23 E. V. Kazarovets *et al.*, *Information Bulletin on Variable Stars*, **4659**, 1, 1999.
24 S. J. Williams, *AJ*, **137**, 3222, 2009.
25 G. Pojmański, *AcA*, **47**, 467, 1997.
26 G. Pojmański, *AcA*, **52**, 397, 2002.
27 J. A. Orosz & P. H. Hauschildt, *A&A*, **364**, 265, 2000.
28 A. J. Cannon & E. C. Pickering, *Annals of Harvard College Observatory*, **92**, 1, 1918.
29 E. Høg *et al.*, *A&A*, **355**, L27, 2000.
30 Gaia Collaboration *et al.*, *A&A*, **649**, A1, 2021.
31 K. G. Stassun *et al.*, *AJ*, **158**, 138, 2019.
32 R. M. Cutri *et al.*, *2MASS All Sky Catalogue of Point Sources* (The IRSA 2MASS All-Sky Point Source Catalogue, NASA/IPAC Infrared Science Archive, Caltech, US), 2003.
33 G. R. Ricker *et al.*, *Journal of Astronomical Telescopes, Instruments, and Systems*, **1**, 014003, 2015.
34 J. M. Jenkins *et al.*, in *Proc. SPIE*, 2016, *Society of Photo-Optical Instrumentation Engineers (SPIE) Conference Series*, vol. 9913, p. 99133E.
35 J. Southworth, P. F. L. Maxted & B. Smalley, *MNRAS*, **351**, 1277, 2004.
36 J. Southworth, *A&A*, **557**, A119, 2013.
37 J. Eastman, R. Siverd & B. S. Gaudi, *PASP*, **122**, 935, 2010.
38 J. Southworth & D. M. Bowman, *MNRAS, submitted*, 2022.
39 D. W. Kurtz, *MNRAS*, **213**, 773, 1985.
40 A. Stankov & G. Handler, *ApJS*, **158**, 193, 2005.
41 C. Waelkens, *A&A*, **246**, 453, 1991.
42 C. Aerts, J. Christensen-Dalsgaard & D. W. Kurtz, *Asteroseismology* (Astron. and Astroph. Library, Springer Netherlands, Amsterdam), 2010.
43 R. E. Wilson & E. J. Devinney, *ApJ*, **166**, 605, 1971.
44 R. E. Wilson, *ApJ*, **234**, 1054, 1979.
45 J. Southworth *et al.*, *MNRAS*, **414**, 2413, 2011.
46 J. Southworth & J. V. Clausen, *A&A*, **461**, 1077, 2007.
47 K. Pavlovski *et al.*, *MNRAS*, **400**, 791, 2009.
48 K. Pavlovski, J. Southworth & E. Tamajo, *MNRAS*, **481**, 3129, 2018.
49 R. E. Wilson & W. Van Hamme, *Computing Binary Star Observables (Wilson-Devinney program user guide), available at ftp://ftp.astro.ufl.edu/pub/wilson*, 2004.
50 J. Zahn, *A&A*, **41**, 329, 1975.
51 J. Zahn, *A&A*, **57**, 383, 1977.
52 A. Claret, *MNRAS*, **327**, 989, 2001.
53 J. Southworth, *MNRAS*, **417**, 2166, 2011.
54 H. Lehmann *et al.*, *A&A*, **557**, A79, 2013.
55 J. Southworth *et al.*, *MNRAS*, **497**, L19, 2020.
56 A. Claret, *A&AS*, **131**, 395, 1998.
57 R. E. Wilson, *ApJ*, **356**, 613, 1990.
58 T. Van Reeth *et al.*, *A&A, in press* `arXiv:2201.05359`, 2022.
59 W. Van Hamme, *AJ*, **106**, 2096, 1993.
60 J. Southworth, P. F. L. Maxted & B. Smalley, *A&A*, **429**, 645, 2005.

61 L. Girardi *et al.*, *A&A*, **391**, 195, 2002.
62 R. Lallement *et al.*, *A&A*, **561**, A91, 2014.
63 R. Lallement *et al.*, *A&A*, **616**, A132, 2018.
64 A. Prša *et al.*, *AJ*, **152**, 41, 2016.
65 J. Southworth, in *Living Together: Planets, Host Stars and Binaries* (S. M. Rucinski, G. Torres & M. Zejda, eds.), 2015, *Astronomical Society of the Pacific Conference Series*, vol. 496, p. 321.
66 A. Bressan *et al.*, *MNRAS*, **427**, 127, 2012.
67 N. Grevesse & A. J. Sauval, *Space Science Rev.*, **85**, 161, 1998.
68 M. Asplund *et al.*, *ARA&A*, **47**, 481, 2009.
69 E. Magg *et al.*, *A&A, in press,* `arXiv:2203.02255`, 2022.
70 M. J. Pecaut & E. E. Mamajek, *ApJS*, **208**, 9, 2013.
71 O. R. Pols *et al.*, *MNRAS*, **298**, 525, 1998.
72 A. Pietrinferni *et al.*, *ApJ*, **612**, 168, 2004.
73 T. Lejeune & D. Schaerer, *A&A*, **366**, 538, 2001.
74 G. Schaller *et al.*, *A&AS*, **96**, 269, 1992.